

Toward the Natural and Realistic NMSSM with and without R -Parity

Taoli Cheng,¹ Jinmian Li,¹ Tianjun Li,^{1,2} Xia Wan,³ You kai Wang,¹ and Shou-hua Zhu^{3,4}

*¹State Key Laboratory of Theoretical Physics and Kavli Institute for
Theoretical Physics China (KITPC), Institute of Theoretical Physics,
Chinese Academy of Sciences, Beijing 100190, P. R. China*

*²George P. and Cynthia W. Mitchell Institute for Fundamental Physics and Astronomy,
Texas A&M University, College Station, TX 77843, USA*

*³Institute of Theoretical Physics & State Key
Laboratory of Nuclear Physics and Technology,
Peking University, Beijing 100871, P. R. China*

⁴Center for High Energy Physics, Peking University, Beijing 100871, P. R. China

Abstract

From the current ATLAS and CMS results on Higgs boson mass and decay rates, the NMSSM is obviously better than the MSSM. To explain the fine-tuning problems such as gauge hierarchy problem and strong CP problem in the SM, we point out that supersymmetry does not need to provide a dark matter candidate, *i.e.*, R -parity can be violated. Thus, we consider three kinds of the NMSSM scenarios: in Scenarios I and II R -parity is conserved and the lightest neutralino relic density is respectively around and smaller than the observed value, while in Scenario III R -parity is violated. To fit all the experimental data, we consider the χ^2 analyses, and find that the Higgs boson mass and decay rates can be explained very well in these Scenarios. Considering the small χ^2 values and fine-tuning around 2-3.7% (or 1-2%), we obtain the viable parameter space with light (or relatively heavy) supersymmetric particle spectra only in Scenario III (or in Scenarios I and II). Because the singlino, Higgsinos, and light stop are relatively light in general, we can relax the LHC supersymmetry search constraints but the XENON100 experiment gives a strong constraint in Scenarios I and II. In all the viable parameter space, the anomalous magnetic moment of the muon $(g_\mu - 2)/2$ are generically small. With R -parity violation, we can increase $(g_\mu - 2)/2$, and avoid the constraints from the LHC supersymmetry searches and XENON100 experiment. Therefore, Scenario III with R -parity violation is more natural and realistic than Scenarios I and II.

PACS numbers: 11.10.Kk, 11.25.Mj, 11.25.-w, 12.60.Jv

I. INTRODUCTION

The Higgs boson mass in the Standard Model (SM) is not stable against quantum corrections and its square has quadratic divergences. Because the reduced Planck scale is about 16 order larger than the electroweak (EW) scale, there exists huge fine-tuning around 10^{-32} to obtain the EW-scale Higgs boson mass. Supersymmetry is a symmetry between the bosonic and fermionic states, and it naturally solves this problem due to the cancellations between the bosonic and fermionic quantum corrections. In Minimal Supersymmetric SM (MSSM), the gauge couplings for $SU(3)_C$, $SU(2)_L$ and $U(1)_Y$ gauge symmetries are unified at about 2×10^{16} GeV [1], which strongly suggests Grand Unified Theories (GUTs). Unlike the SM, we can have the renormalizable superpotential terms that violate the baryon and lepton numbers, and then there may exist proton decay problem. To solve such problem, we usually introduce the R -parity under which the SM particles are even while the extra supersymmetric particles (sparticles) are odd. Thus, the lightest supersymmetric particle (LSP) like neutralino can be cold dark matter candidate [2, 3].

However, there are strong constraints on the supersymmetry viable parameter space from the recent LHC supersymmetry searches [4–8]. For example, in the Minimal Supergravity (mSUGRA) model or Constrained MSSM (CMSSM), gluino mass should be larger than about 1.4 TeV and 850 GeV for squark masses around and much larger than gluino mass, respectively. Also, squarks (at least the first two generation squarks) must have masses larger than about 1.1 TeV from the ATLAS and CMS Collaborations at the LHC [4–8].

Recently, the ATLAS and CMS Collaborations have announced the discovery of a Higgs-like boson with mass around 126.5 GeV and 125.3 ± 0.6 GeV, respectively [9–11]. In the $\gamma\gamma$ final state, the ATLAS and CMS rates are roughly 1.9 ± 0.5 and 1.56 ± 0.43 times the SM prediction. In the $ZZ \rightarrow 4\ell$ channel, the ATLAS and CMS signals are roughly $1.1^{+0.5}_{-0.4}$ and $0.7^{+0.4}_{-0.3}$ times the SM prediction, respectively. In the $b\bar{b}$, $\tau^+\tau^-$ and $WW \rightarrow \ell\nu\ell\nu$ channels, the ATLAS rates are respectively $0.48^{+2.17}_{-2.12}$, $0.16^{+1.72}_{-1.84}$, and $0.52^{+0.57}_{-0.60}$ times the SM prediction, and the CMS rates are respectively $0.15^{+0.73}_{-0.66}$, $-0.14^{+0.76}_{-0.73}$, and $0.62^{+0.43}_{-0.45}$. So these rates are somewhat suppressed compare to the SM prediction but error bars are relatively large. The Higgs physics implications in the supersymmetric SMs (SSMs) have been studied extensively [12–16]. By the way, the new results from the CDF and D0 experiments [17] support the ~ 125 GeV Higgs signal and suggest an enhancement relative to the SM of the

W +Higgs with $\text{Higgs} \rightarrow b\bar{b}$ rate by a factor of $1.97^{+0.74}_{-0.68}$. But we will consider not it here since it is different from the ATLAS and CMS results.

As we know, there are two Higgs doublets H_u and H_d in the MSSM that gives masses to the up-type quarks and down-type quarks/charged leptons, respectively. The lightest CP-even Higgs boson mass, which is a linear combination of H_u^0 and H_d^0 and usually SM-like, is smaller than Z boson mass M_Z at tree level. Thus, to realize the lightest CP-even Higgs boson mass around 125.5 GeV radiatively, the squark and/or gluino masses will be about a few TeV in general in the mSUGRA/CMSSM. And then there exists at least less than one-percent fine-tuning. Moreover, it is difficult to explain the above Higgs decay rates and generate the correct Higgs boson mass simultaneously in the MSSM. For example, if the SM-like Higgs particle has dominant component from H_u^0 , we can suppress the rates in the $b\bar{b}$ and $\tau^+\tau^-$ final states, and then increase the $\gamma\gamma$ rate. But the rates for the $ZZ \rightarrow 4\ell$ and $WW \rightarrow \ell\nu\ell\nu$ channels will increase as well. Also, if the stop is light, we can increase the Higgs to two photon rate, but it is difficult to generate the 125.5 GeV Higgs boson mass [12–16]. The possible model might be the light stau scenario [13]. Therefore, we shall consider the next to the MSSM (NMSSM) where an SM singlet field S is introduced. The points are the following: (1) We can increase the Higgs quartic coupling from the superpotential term $\lambda SH_d H_u$ if the ratio $\tan\beta \equiv \langle H_u^0 \rangle / \langle H_d^0 \rangle$ of the vacuum expectation values (VEVs) for H_u^0 and H_d^0 is not large; (2) We can suppress the couplings between the W/Z gauge bosons and the Higgs particle due to the mixings among S , H_u^0 , and H_d^0 .

On the other hand, the strong CP problem is another big fine-tuning problem in the SM. From the experimental bound on the neutron electric dipole moment (EDM), the strong CP phase $\bar{\theta}$ is required to be smaller than 10^{-10} . An elegant and popular solution to the strong CP problem is provided by the Peccei–Quinn (PQ) mechanism [18], in which a global axial symmetry $U(1)_{PQ}$ is introduced and broken spontaneously at some high energy scale. The axion a is a pseudo-Goldstone boson from the spontaneous $U(1)_{PQ}$ symmetry breaking, with a decay constant f_a . The original Weinberg–Wilczek axion [19] is excluded by experiment, in particular by the non-observation of the rare decay $K \rightarrow \pi + a$ [20]. There are two viable “invisible” axion models in which the experimental bounds can be evaded: the Kim–Shifman–Vainshtein–Zakharov (KSVZ) axion model [21] and the Dine–Fischler–Srednicki–Zhitnitskii (DFSZ) axion model [22]. From laboratory, astrophysics, and cosmological constraints, the $U(1)_{PQ}$ symmetry breaking scale f_a is constrained to the range

$10^{10} \text{ GeV} \leq f_a \leq 10^{12} \text{ GeV}$ [20]. Interestingly, for such f_a range, the invisible axion can be a good cold dark matter candidate with correct relic density [20].

Because axion can be the correct dark matter candidate, supersymmetry may only need to solve the gauge hierarchy problem and realize gauge coupling unification. Therefore, we consider three kinds of the NMSSM scenarios: in Scenario I, R -parity is conserved and the LSP neutralino relic density is around the observed value; in Scenario II, R -parity is conserved and the LSP neutralino relic density is smaller than the observed value; in Scenario III, R -parity is violated and then the LSP neutralino is not stable. In particular, Scenario III is very interesting since it can not only avoid the constraints from the LHC supersymmetry searches and XENON100 experiment [23], but also may relax the other phenomenological constraints. Moreover, the proton decay problem can be solved by requiring the baryon or lepton number conservation [24], or by requiring the minimal flavour violation [25].

In this paper, we shall study the natural and realistic NMSSM. We first briefly review the naturalness condition in the SSMs and discuss the NMSSM with and without R -parity. To satisfy the phenomenological constraints and fit the experimental data, we consider the χ^2 analyses for all three kinds of Scenarios, and find that we can indeed explain the Higgs boson mass and decay rates very well. Considering the small χ^2 values and fine-tuning around 2-3.7%, we obtain the viable parameter space with light (e.g. less than around 900 GeV) supersymmetric particle spectra only in Scenario I. For the small χ^2 values and fine-tuning around 1-2%, we get the viable parameter space with relatively heavy (e.g. less than about 1.2 TeV) supersymmetric particle spectra. In particular, the best benchmark point has almost minimal χ^2 and 3.7% fine-tuning in Scenario III. The generic features for the viable parameter space with smaller χ^2 are that the light stop is around 500 GeV or smaller, the singlino and Higgsino are light chargino and neutralinos, the Wino-like chargino is heavy, and the Bino-like and Wino-like neutralinos are the second heaviest neutralino and heaviest neutralinos, respectively. Thus, we find that the LHC supersymmetry search constraints can be relaxed due to quite a few jets and/or leptons in the final states in Scenarios I and II, but the XENON100 experiment still gives strong constraint on the dark matter direct detection cross sections. Moreover, the correct dark matter relic density can be realized in Scenario I as well. In particular, $\tan\beta$ is not large and the second lightest CP-even Higgs particle is SM-like [14, 16], which is helpful to increase the SM-like Higgs boson mass. However, the additional contributions to the anomalous magnetic moment of the muon $(g_\mu - 2)/2$

are smaller than three sigma low bound [26] in general due to relatively small $\tan\beta$. As we know, with R -parity violation, we can escape the constraints from the LHC supersymmetry searches and XENON100 experiment, and the R -parity violation superpotential term(s) may increase the muon $(g_\mu - 2)/2$ and explain the neutrino masses and mixings. Therefore, Scenario III with R -parity violation is more natural and realistic than Scenarios I and II.

This paper is organized as follows. We explain the naturalness criteria in the SSMs in Section II. We present the NMSSM with and without R -parity in Section III, and the experimental constraints/data and numerical analyses in Section IV. Section V is our conclusion.

II. NATURALNESS CRITERIA IN THE SSMs

For the GUTs with gravity mediated supersymmetry breaking, the usual quantitative measure Δ_{FT} for fine-tuning is the maximum of the logarithmic derivative of M_Z with respect to all the fundamental parameters a_i at the GUT scale [27]

$$\Delta_{\text{FT}} = \text{Max}\{\Delta_i^{\text{GUT}}\}, \quad \Delta_i^{\text{GUT}} = \left| \frac{\partial \ln(M_Z)}{\partial \ln(a_i^{\text{GUT}})} \right|. \quad (1)$$

In the following numerical calculations, we will use this definition to calculate the fine-tuning.

However, the above fine-tuning definition is a little bit abstract. Thus, we shall present the concrete bounds on the μ term, third-generation squark masses and gluino mass in the following [28, 29]. The SM Higgs-like particle h in the MSSM is a linear combination of H_u^0 and H_d^0 . To simplify the discussion on naturalness, we can reduce the Higgs potential to

$$V = \overline{m}_h^2 |h|^2 + \frac{\lambda_h}{4} |h|^4, \quad (2)$$

where \overline{m}_h^2 is negative. Minimizing the Higgs potential, we get the physical SM-like Higgs boson mass m_h

$$m_h^2 = -2\overline{m}_h^2. \quad (3)$$

So the fine-tuning measure can also be defined as [28]

$$\Delta_{\text{FT}} \equiv \frac{2\delta\overline{m}_h^2}{m_h^2}. \quad (4)$$

For a moderately large $\tan\beta \equiv \langle H_u^0 \rangle / \langle H_d^0 \rangle$, for instance, $\tan\beta \geq 2$, we have

$$\overline{m}_h^2 \simeq |\mu|^2 + m_{H_u}^2|_{\text{tree}} + m_{H_u}^2|_{\text{rad}}, \quad (5)$$

where μ is the supersymmetric bilinear mass between H_u and H_d , and $m_{H_u}^2|_{\text{tree}}$ and $m_{H_u}^2|_{\text{rad}}$ are the tree-level and radiative contributions to the soft supersymmetry-breaking mass squared for H_u . Therefore, we obtain the following concrete bounds [29]:

- The upper bound on the μ term is

$$\mu \lesssim 400 \text{ GeV} \left(\frac{m_h}{125.5 \text{ GeV}} \right) \left(\frac{\Delta_{\text{FT}}^{-1}}{5\%} \right)^{-1/2}. \quad (6)$$

Thus, the μ term should be small than about 400 GeV for 5% fine-tuning. Consequently, the charged and neutral Higgsinos will be light. In the NMSSM, we just change the μ term to the effective μ term $\mu_{\text{eff}} \equiv \lambda \langle S \rangle$.

- The one-loop radiative corrections to $m_{H_u}^2$ in the leading logarithmic approximation from the stop sector are

$$\delta m_{H_u}^2|_{\text{stop}} = -\frac{3}{8\pi^2} y_t^2 \left(m_{\tilde{Q}_3}^2 + m_{\tilde{U}_3^c}^2 + |A_t|^2 \right) \ln \left(\frac{\Lambda}{\text{TeV}} \right), \quad (7)$$

where y_t is top Yukawa coupling, $m_{\tilde{Q}_3}^2$ and $m_{\tilde{U}_3^c}^2$ are supersymmetry breaking soft masses for the third generation quark doublet and right-handed stop, A_t is the top trilinear soft term, and Λ is the effective supersymmetry breaking mediation scale. Thus, one obtains

$$\sqrt{m_{\tilde{t}_1}^2 + m_{\tilde{t}_2}^2} \lesssim 1.2 \text{ TeV} \frac{\sin \beta}{(1 + x_t^2)^{1/2}} \left(\frac{\ln(\Lambda/\text{TeV})}{3} \right)^{-1/2} \left(\frac{m_h}{125.5 \text{ GeV}} \right) \left(\frac{\Delta_{\text{FT}}^{-1}}{5\%} \right)^{-1/2}, \quad (8)$$

where $x_t = A_t / \sqrt{m_{\tilde{t}_1}^2 + m_{\tilde{t}_2}^2}$, and \tilde{t}_1 and \tilde{t}_2 are two stop mass eigenstates. Therefore, we obtain $\sqrt{m_{\tilde{t}_1}^2 + m_{\tilde{t}_2}^2} \leq 1.2 \text{ TeV}$. Also, we can require that the lighter sbottom mass be smaller than $m_{\tilde{t}_2}$, which is automatically satisfied via an simple mathematical proof.

- The two-loop radiative corrections to $m_{H_u}^2$ in the leading logarithmic approximation from gluino are

$$\delta m_{H_u}^2|_{\text{gluino}} = -\frac{2}{\pi^2} y_t^2 \left(\frac{\alpha_s}{\pi} \right) |M_3|^2 \ln^2 \left(\frac{\Lambda}{\text{TeV}} \right), \quad (9)$$

where α_s is the strong coupling, and M_3 is the gluino mass. Here, the contributions from the mixed $A_t M_3$ term, which are relevant for large A-term, are neglected. Thus, the bound on gluino mass is

$$M_3 \lesssim 1.8 \text{ TeV} \sin \beta \left(\frac{\ln(\Lambda/\text{TeV})}{3} \right)^{-1} \left(\frac{m_h}{125.5 \text{ GeV}} \right) \left(\frac{\Delta_{\text{FT}}^{-1}}{5\%} \right)^{-1/2}. \quad (10)$$

So the gluino mass is lighter than about 1.8 TeV.

Therefore, the natural MSSM and NMSSM should have relatively smaller (effective) μ term, stop masses as well as gluino mass. In this paper, we shall not only use Eq. (1) to calculate the numerical values of the fine-tuning, but also consider the following natural supersymmetry conditions:

- The μ term or effective μ term is smaller than 300 GeV.
- The squar root $M_{\tilde{t}} \equiv \sqrt{m_{\tilde{t}_1}^2 + m_{\tilde{t}_2}^2}$ of the sum of the two stop mass squares is smaller than 1.2 TeV. Consequencely, we can show that the light sbottom mass is smaller than $m_{\tilde{t}_2}$.
- The gluino mass is lighter than 1.5 TeV.

However, such kind of the natural MSSM and NMSSM might be excluded by the LHC supersymmetry searches and XENON100 dark matter direct detection. Thus, the R -parity violation might be needed for the natural MSSM and NMSSM, and then supersymmetry only needs to solve the fine-tuning problem and explain the gauge coupling unification.

III. THE NMSSM WITH AND WITHOUT R -PARITY

Let us explain the convention first. We denote the quark doublets, right-handed up-type quarks, right-handed down-type quarks, lepton doublets, and right-handed leptons as Q_i , U_i^c , D_i^c , L_i , and E_i^c , respectively. We denote the $SU(3)_C$, $SU(2)_L$, and $U(1)_Y$ gauginos as \tilde{G}^a , \tilde{W}^a , and \tilde{B} , respectively. To solve the μ problem in the MSSM, we introduce a SM singlet field S and consider the NMSSM with Z_3 symmetry which forbids the μ term. The superpotential in the NMSSM is

$$W_{\text{NMSSM}} = y_{ij}^u Q_i U_j^c H_u + y_{ij}^d Q_i D_j^c H_d + y_{ij}^l L_i E_j^c H_d + \lambda S H_d H_u + \frac{1}{3} \kappa S^3, \quad (11)$$

where y_{ij}^u , y_{ij}^d , y_{ij}^l , λ , and κ are Yukawa couplings. The effective μ term is obtained after S obtains a VEV, *i.e.*, $\mu_{\text{eff}} \equiv \lambda \langle S \rangle$.

The supersymmetry breaking soft terms are

$$\begin{aligned}
-\mathcal{L} = & \frac{1}{2} \left[M_1 \tilde{B} \tilde{B} + M_2 \sum_{a=1}^3 \tilde{W}^a \tilde{W}_a + M_3 \sum_{a=1}^8 \tilde{G}^a \tilde{G}_a + \text{H.C.} \right] + m_{H_u}^2 |H_u|^2 + m_{H_d}^2 |H_d|^2 \\
& + m_S^2 |S|^2 + m_{\tilde{Q}_i}^2 |\tilde{Q}_i|^2 + m_{\tilde{U}_i^c}^2 |\tilde{U}_i^c|^2 + m_{\tilde{D}_i^c}^2 |\tilde{D}_i^c|^2 + m_{\tilde{L}_i}^2 |\tilde{L}_i|^2 + m_{\tilde{E}_i^c}^2 |\tilde{E}_i^c|^2 \\
& + \left[y_{ij}^u A_{ij}^u Q_i U_j^c H_u + y_{ij}^d A_{ij}^d Q_i D_j^c H_d + y_{ij}^l A_{ij}^l L_i E_j^c H_d + \lambda A_\lambda S H_d H_u \right. \\
& \left. + \frac{1}{3} \kappa A_\kappa S^3 + \text{H.C.} \right] .
\end{aligned} \tag{12}$$

Similar to the MSSM, the Higgs sector of the NMSSM is described by the following six parameters

$$\lambda, \kappa, A_\lambda, A_\kappa, \tan \beta, \mu_{\text{eff}} . \tag{13}$$

And the supersymmetry breaking soft mass terms for the Higgs bosons $m_{H_u}^2$, $m_{H_d}^2$ and m_S^2 are determined implicitly by M_Z , $\tan \beta$ and μ_{eff} via the Higgs potential minimization.

In addition, from the theoretical point of view, we usually have the family universal squark and slepton soft masses in the string model building. Therefore, as in the mSUGRA/CMSSM, we consider the following universal supersymmetry breaking soft terms

$$M_1 = M_2 = M_3 \equiv M_{1/2} , \tag{14}$$

$$m_{\tilde{Q}_i}^2 = m_{\tilde{U}_i^c}^2 = m_{\tilde{D}_i^c}^2 = m_{\tilde{L}_i}^2 = m_{\tilde{E}_i^c}^2 \equiv M_0^2 , \tag{15}$$

$$A_{ij}^u = A_{ij}^d = A_{ij}^l \equiv A_0 . \tag{16}$$

We consider the NUH-NMSSM in this paper: the Higgs soft mass terms $m_{H_u}^2$, $m_{H_d}^2$ and m_S^2 are allowed to be different from M_0^2 (and determined implicitly as mentioned above), and the trilinear couplings A_λ , A_κ and A_0 are not universal. Therefore, the complete parameter space is characterized by

$$\lambda, \kappa, \tan \beta, \mu_{\text{eff}}, A_\lambda, A_\kappa, A_0, M_{1/2}, M_0 , \tag{17}$$

where the last five parameters are taken at the GUT scale.

Next, we consider the R -parity violation. The most general renormalizable, gauge and Z_3 invariant, and R -parity odd superpotential terms in the NMSSM are [24]

$$W_{\text{RPV}} = \lambda_i S L_i H_u + \frac{1}{2} \lambda_{ijk} L_i L_j E_k^c + \lambda'_{ijk} L_i Q_j D_k^c + \frac{1}{2} \lambda''_{ijk} U_i^c D_j^c D_k^c , \tag{18}$$

where λ_i , λ_{ijk} , λ'_{ijk} , and λ''_{ijk} are Yukawa couplings. In the above Eq. (18), the first three terms conserve the baryon number while violate the lepton number, and the last term conserves the lepton number while violates the baryon number. Thus, to forbid the proton decay, we require either baryon number conservation or lepton number conservation, *i.e.*, we turn on either the first three terms or the last term in the above superpotential [24]. The alternative ways are to consider the minimal flavour violation [25] or discrete Z_N R -symmetry [30]. In particular, the λ_{ijk} and λ'_{ijk} terms can contribute to the anomalous magnetic moment of the muon $(g_\mu - 2)/2$ and generate the neutrino masses and mixings, and the λ'_{ijk} and λ''_{ijk} terms can contribute to the $b \rightarrow s\gamma$, etc [24]. We would like to point out that the NMSSM with R -parity violation has been studied before [31], and the NMSSM with baryon number conservation is similar to the $\mu\nu$ SSM [32].

In this paper, to increase the SM-like Higgs boson mass while keep the sparticle spectrum light, we will concentrate on the natural and realistic NMSSM with the following properties: (1) $\tan\beta$ is not large so that the SM-like Higgs boson mass can be lifted via the tree-level $\lambda SH_d H_u$ term; (2) The second lightest CP-even Higgs boson is the SM-like Higgs particle, and then the SM-like Higgs boson mass can be lifted via the mass matrix diagonalization from Linear Algebra. However, in such kind of viable parameter space, the muon $(g_\mu - 2)/2$ is generically small due to not large $\tan\beta$. Thus, to increase muon $(g_\mu - 2)/2$, we need to introduce R -parity violation λ_{ijk} and λ'_{ijk} terms in Eq. (18), which will be studied elsewhere. Interestingly, we may explain the neutrino masses and mixings simultaneously.

IV. χ^2 ANALYSES FOR THE PHENOMENOLOGICAL CONSTRAINTS AND EXPERIMENTAL DATA

We will consider the χ^2 analyses for the phenomenological constraints and experimental data in all three scenarios. For our numerical calculations, we use the NMSSMTools version 3.2.0 [33].

In the original package, the points are survived if they satisfy several phenomenological and theoretical constraints. Two standard deviation (95% C.L. upper) limits are applied for those constraints which have corresponding experimental measurements. In this paper, these two standard deviation (95% C.L. upper) limits are replaced by their central values and the experimental errors, which are used to construct the global χ^2 . There are two

advantages for this global fit: (1) The best-fitted benchmark points with minimal χ^2 value can be found exactly, while the previous method within two standard deviation limits can only provide a viable parameter space. (2) The derivation for the central values in the two standard deviation limits can accumulate to be a relatively significant drift while the global χ^2 can have explicit statistical meanings for the 1 or 2 standard deviations from the best-fitted points.

In our analyses, several phenomenological and theoretical constraints are considered. These constraints can be divided into the following categories:

1. The theoretical constraints and phenomenological constraints, which only have 95% C.L. upper limits, are unchanged in the NMSSMTools ¹.
2. The following LHC Higgs constraints are added: the second CP-even neutral Higgs field H_2 are taken as the SM-like Higgs boson discovered at the LHC and its mass is required to be $M_{H_2} \in [124, 127]$ GeV. All the 5 neutral Higgs fields H_1, H_2, H_3, A_1 and A_2 should satisfy the LHC constraints, which are taken as the 95% C.L. on $\sigma/\sigma_{\text{SM}}$ among the LHC measured Higgs mass regions. Table I shows the ATLAS and CMS Higgs decay channels that we will consider.

TABLE I: The LHC collider constraints at 95% C.L. on $\sigma/\sigma_{\text{SM}}$. 7, 8 and 7&8 means LHC center mass energy $\sqrt{S} = 7, 8$ TeV as well as 7 and 8 TeV combined results. The blank means no constraints in this channel. Same conventions are applied in the following tables. “(VH)” in the table indicates the experimental results are actually measured in the vector boson associated production, which is invariant for the WH production channel in the NMSSM.

¹ For interested readers, the detailed information can be found in NMSSMTOOLS 3.2.0, which corresponds to PROB(1)~PROB(29), PROB(35), PROB(41)~PROB(45), PROB(51) and PROB(52).

Channels	ATLAS	CMS
$H \rightarrow \tau\tau$		7, 7&8
$WH \rightarrow bb$		7, 7&8(VH)
$H \rightarrow bb$		
$H \rightarrow ZZ$	7, 8, 7&8	7, 7&8
$H \rightarrow W^+W^-$		7, 7&8
$H \rightarrow \gamma\gamma$	7, 8, 7&8	7, 7&8
$2jH \rightarrow 2j\gamma\gamma$		

3. The NMSSMTools two standard deviation constraints are replaced by global χ^2 fits, which include: $b \rightarrow s\gamma$, δm_s , δm_d , $b \rightarrow \tau\nu_\tau$, $(g_\mu - 2)/2$ and $\text{Br}(B \rightarrow X_s\mu^+\mu^-)$. We update the anomalous magnetic moment of the muon $(g_\mu - 2)/2$: $\Delta a_\mu = a_\mu^{\text{exp}} - a_\mu^{\text{SM}} = (28.7 \pm 8.0) \times 10^{-10}$ [26].
4. LHC Higgs signal strength is constructed in the χ^2 , as shown in Table II and Fig. 1. Theoretical predictions in the χ^2 correspond to H_2 in the NMSSM. For the 7 and 8 TeV combined results, the theoretical predicted signal strength for inclusive Higgs production channels are combined from the 7 and 8 TeV individual signal strength proportional to their accumulated luminosities.

TABLE II: LHC Higgs signal strength in χ^2 .

Channels	ATLAS	CMS
$H \rightarrow \tau\tau$	7	7&8
$WH \rightarrow bb$	7	7&8(VH)
$H \rightarrow bb$	7	7&8
$H \rightarrow ZZ$	7&8	7&8
$H \rightarrow W^+W^-$	7	7&8
$H \rightarrow \gamma\gamma$	7&8	7&8
$2jH \rightarrow 2j\gamma\gamma$	7&8	7&8

5. The cold dark matter relic density is 0.112 ± 0.0056 from the seven-year WMAP measurements [34]. For the dark matter, we treat it in three different scenarios, as

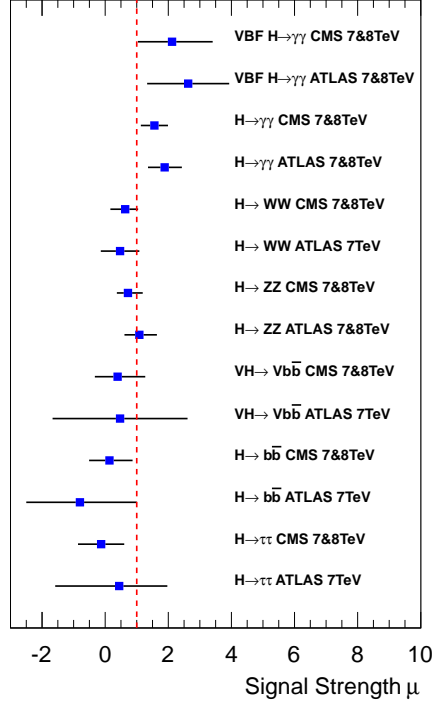


FIG. 1: LHC Higgs signal strength in different production and decay modes.

shown in the Table III. In Scenario I, the lightest stable neutralino is required to have the correct dark matter relic density. This is considered in the global χ^2 . In Scenario II, the relic density is required to be smaller than the 95% C.L. experimental upper limit, which assumes multi-component dark matter. In Scenario III, the relic density is set to be free, which corresponds to the R -parity violation case. Constraints of effective Higgs self-couplings in MicrOMEGAs and spin independent dark matter direct detection of XENON100 experiment [23] in the NMSSMTools package are adjusted according to different relic density treatment as shown in Table III.

TABLE III: Three different dark matter relic density scenarios.

	scenario I	scenario II	scenario III
Ωh^2	in χ^2	< 95%upper limit	free
Effective Higgs Self-Coupling in MicrOMEGAs > 1	✓	✓	×
XENON100	✓	✓	×

To be clear, we have considered three scenarios according to the different dark matter treatments as explained in category 5. Categories 1 to 4 are common constraints that are applied to all three Scenarios.

The χ^2 is constructed as:

$$\chi^2 = \sum_i \left(\frac{\mu_i^{the} - \mu_i^{exp}}{\delta_i} \right)^2, \quad (19)$$

in which μ_i^{the} are theoretical predicted values and μ_i^{exp} are corresponding experimental measurements. δ_i are one standard fluctuations which includes both statistical and systematical errors and are taken as the average values for asymmetric errors.

By adopting the above χ^2 constructions, the number of independent variables in the χ^2 are: 7 in category 3 (Br ($B \rightarrow X_s \mu^+ \mu^-$) are considered in both low and high dilepton energy regions), 14 LHC Higgs decay signal strength (we assume that ATLAS and CMS measurements on the same Higgs decay channels are independent), and the different dark matter relic density Scenarios in category 5. Besides, there are 9 NMSSM input parameters as shown in Eq. (17). So the number of degree of freedom n_d is 22-9=13 for Scenario I and 12 for Scenarios II and III. The goodness of fit can be shown by comparing the minimum χ^2 with the n_d .

Note that the current top quark mass m_t is 173.5 ± 1 GeV, we shall choose the central value $m_t = 173.5$ GeV in numerical calculations. We emphasize that the SM-like Higgs boson H_2 mass will increase and decrease about 1 GeV if we choose the upper limit $m_t = 174.5$ GeV and low limit $m_t = 172.5$ GeV, respectively. Thus, the SM-like Higgs boson H_2 mass range from 124 GeV or 127 GeV is fine. Moreover, we define

$$R_i^{X\bar{X}} \equiv \frac{\sigma(pp \rightarrow H_i) \text{BR}(H_i \rightarrow X\bar{X})}{\sigma(pp \rightarrow h_{\text{SM}}) \text{BR}(h_{\text{SM}} \rightarrow X\bar{X})}, \quad (20)$$

where $X\bar{X}$ can be $\gamma\gamma$, $Z^0 Z^0$, $W^+ W^-$, $b\bar{b}$, and $\tau\bar{\tau}$.

We present the R_2^{VV} versus $R_2^{\gamma\gamma}$, $R_2^{\tau\bar{\tau}}$ versus $R_2^{b\bar{b}}$, $M_{\tilde{t}}$ versus $M_{\tilde{g}}$, Δ_{FT} versus χ^2 , $\tan \beta$ versus Δa_μ , $m_{\tilde{t}_1}$ versus μ_{eff} , M_{H_1} versus M_{H_2} , $M_{\tilde{u}}$ versus $M_{\tilde{g}}$, and $M_{\tilde{l}}$ versus $M_{\tilde{\tau}_1}$ in Figs. 2, 3, and 4 for Scenarios I, II, and III, respectively. The red stars show the best-fitted benchmark points with minimal $\chi_{\text{min}}^2 = 21.16, 19.35, 19.67$ for Scenarios I, II, III, respectively. The magenta region corresponds to $R_{\gamma\gamma} > 1.4$, $R_{VV} < 1.1$, $R_{bb} < 1.0$, $R_{\tau\tau} < 1.0$, $M_{\tilde{t}} = \sqrt{m_{\tilde{t}_1}^2 + m_{\tilde{t}_2}^2} < 1.2$ TeV, $\mu_{\text{eff}} < 300$ GeV, $M_{\tilde{g}} < 1.2$ TeV, $\chi^2 < \chi_{\text{min}}^2 + 4$, and $\Delta_{\text{FT}} < 50$. In particular, the small χ^2 and $\Delta_{\text{FT}} < 50$ are not compatible with each other in Scenarios I and II due

to XENON100 experimental constraint, and then only Scenario III has magenta region. In addition to the minimal χ^2 points, we consider three kinds of other benchmark points:

- Benchmark points IA, IIA, and IIIA have small χ^2 , relatively small Δ_{FT} , the light stop mass around 200 GeV, and the first two generation squark masses lighter than about 1.1 TeV.
- Benchmark points IB, IIB, and IIIB have small χ^2 , relatively small Δ_{FT} , the light stop mass around 200 GeV, and the first two generation squark masses heavier than about 1.1 TeV.
- Benchmark points IC, IIC, and IIIC have small χ^2 , relatively small Δ_{FT} , and relatively heavier light stop.

We present the minimal χ^2 point, and three other benchmark points in Tables IV, V, and VI for Scenarios I, II, and III, respectively. Moreover, we study the constraints from the LHC supersymmetry searches, and find that only the benchmark points IA and IIA are excluded by the current LHC supersymmetry searches [4–8]. Because the benchmark points $\text{I}\chi_{\text{min}}^2$, IC, IIB and IIC have relatively light spectra (e.g. less than about 1.2 TeV), the LHC supersymmetry search constraints are relaxed in our models, which will be explained briefly in the following. The benchmark points in Scenarios I and II have fine-tuning from about 1% to 2%, while the benchmark points in Scenario III have fine-tuning from about 2% to 3.7%. In particular, in the best benchmark point IIIA we have $\chi^2 = 21.31$, and $\Delta_{\text{FT}} = 27.0$, *i.e.*, 3.7% fine-tuning. Also, all the supersymmetric particles are lighter than 830 GeV. By the way, all the benchmark points except $\text{II}\chi_{\text{min}}^2$ satisfy the naturalness conditions: $\mu_{\text{eff}} < 300$ GeV, $M_{\tilde{t}} < 1.2$ TeV, and $M_{\tilde{g}} \leq 1.5$ TeV. Note that $\Delta_{\text{FT}} = 130.4$ in benchmark point $\text{II}\chi_{\text{min}}^2$, the two fine-tuning definitions in Section II are compatible.

From the viable parameter space in Figs. 2, 3, and 4, we find that $\tan\beta$ is generically smaller than about 4.5, and then we have the small anomalous magnetic moment of the muon $(g_\mu - 2)/2$, *i.e.*, $\Delta a_\mu < 4.0 \times 10^{-10}$. Also, we notice the correlation between $R_2^{\gamma\gamma}$ and R_2^{VV} which roughly is $R_2^{\gamma\gamma} \sim 1.27 \times R_2^{VV}$. Interestingly, we do have some viable parameter space which indeed have $R_2^{\gamma\gamma} \geq 1.4$ and $R_2^{VV} \leq 1.1$. The generic features for the parameter space with small χ^2 are that the light stop is around 500 GeV or smaller, the singlino and Higgsino are light neutralinos and chargino, the Wino-like chargino is heavy, and the Bino-like and Wino-like neutralinos are the second heaviest neutralino and the heaviest neutralino,

respectively. Thus, we can understand why the LHC supersymmetry search constraints are relaxed: the branch ratios of the first two generation squarks decaying directly to the LSP neutralino and quarks are very small around 1%, and the dominant decay channels are Wino-like chargino/neutralino and quarks. And then the Wino-like chargino and neutralino will decay into quite a few jets or leptons via the light chargino and neutralinos. Also, gluino will decay dominant into the stop and top quarks, which have long decay chains as well. Therefore, the LHC supersymmetry search constraints can be relaxed. The detailed LHC supersymmetry search constraints will be studied elsewhere. Moreover, because the LSP neutralino has relatively large Higgsino components due to small effective μ term, the XENON100 experiment gives strong constraint, for example, the spin-independent LSP neutralino-nucleon cross sections are larger than the XENON100 experiment upper bound in the benchmark points III χ_{min}^2 , IIIA, and IIIC [23] if R -parity is conserved. This is another reason why we get better points in Scenario III than Scenario II. In Scenario III, the constraints from the LHC supersymmetry searches and XENON100 experiment can be escaped, and the R -parity violating λ_{ijk} and λ'_{ijk} terms can increase $(g_\mu - 2)/2$ and generate the neutrino masses and mixings. Therefore, Scenario III with R -parity violation is more natural and realistic than Scenarios I and II.

V. CONCLUSION

We pointed out that as a solution to the SM fine-tuning problems, supersymmetry needs not to provide the dark matter candidate, *i.e.*, R -parity can be violated. Because the NMSSM can explain the Higgs boson mass and decay rates better than the MSSM, we considered three kinds of the NMSSM scenarios. To satisfy the phenomenological constraints and fit the experimental data, we studied the χ^2 analyses for all three kinds of Scenarios, and showed that the Higgs boson mass and decay rates can indeed be explained very well. For the small χ^2 values and fine-tuning around 2-3.7%, we obtained the viable parameter space with light (e.g. less than about 900 GeV) supersymmetric particle spectra only in Scenario III. With the small χ^2 values and fine-tuning around 1-2%, we got the viable parameter space with relatively heavy (e.g. less than about 1.2 TeV) supersymmetric particle spectra. Especially, the best benchmark point is IIIA, which has almost minimal χ^2 and 3.7% fine-tuning. The correct dark matter density can be realized in Scenario I as well. The

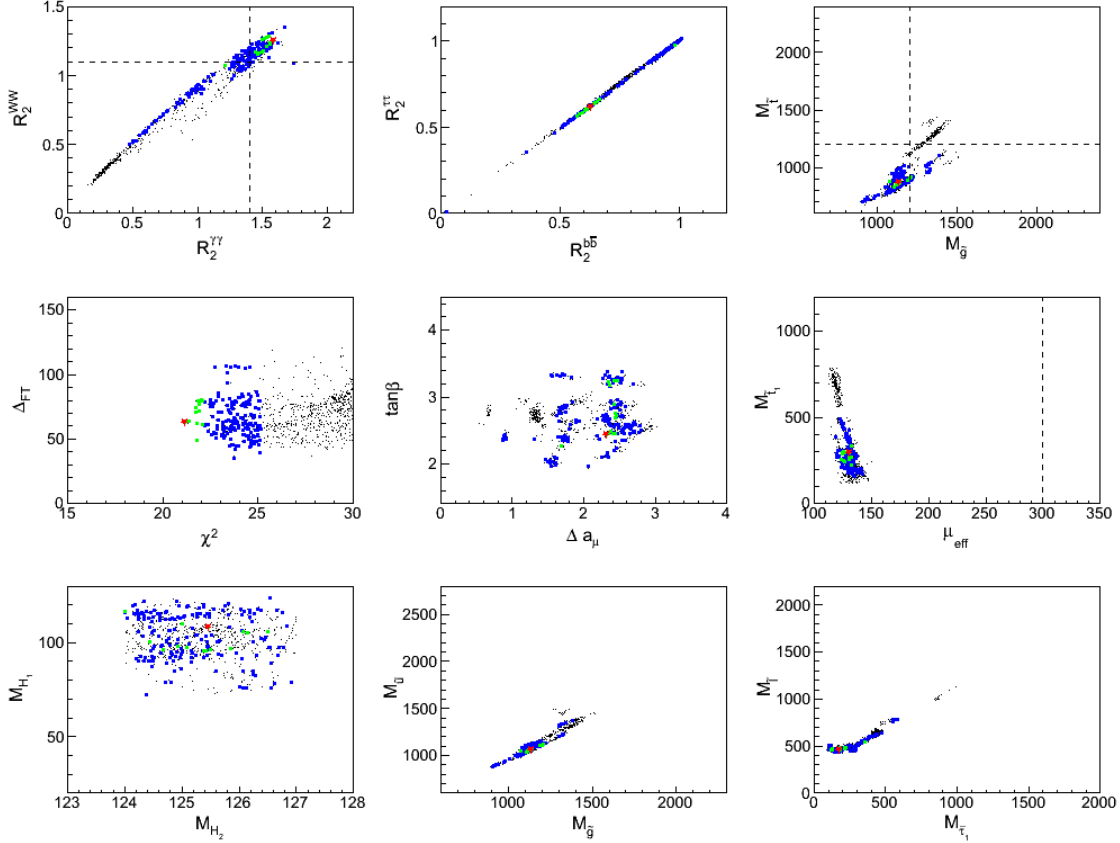


FIG. 2: The fitting results for Scenario I with relic density included in the χ^2 . The red stars show the best-fitted benchmark point with minimal $\chi^2_{min} = 21.16$. The green, blue, and black regions are respectively one, two, and three standard deviation regions with $\chi^2 < \chi^2_{min} + 1, \chi^2_{min} + 4$ and $\chi^2_{min} + 9$.

generic features for the viable parameter space with smaller χ^2 are that the light stop is around 500 GeV or smaller, the singlino and Higgsino are light chargino and neutralinos, the Wino-like chargino is heavy, and the Bino-like and Wino-like neutralinos are the second heaviest neutralino and heaviest neutralinos, respectively. Thus, we found that the LHC supersymmetry search constraints can be relaxed due to quite a few jets and/or leptons in the final states in Scenarios I and II, but the XENON100 experiment still gives strong constraint on the dark matter direct detection cross sections. Moreover, $\tan\beta$ is not large and the second lightest CP-even Higgs particle is SM-like so that the SM-like Higgs boson mass can be lifted. However, the extra contributions to the muon $(g_\mu - 2)/2$ are smaller than three sigma low bound in general due to relatively small $\tan\beta$. With R -parity violation, we

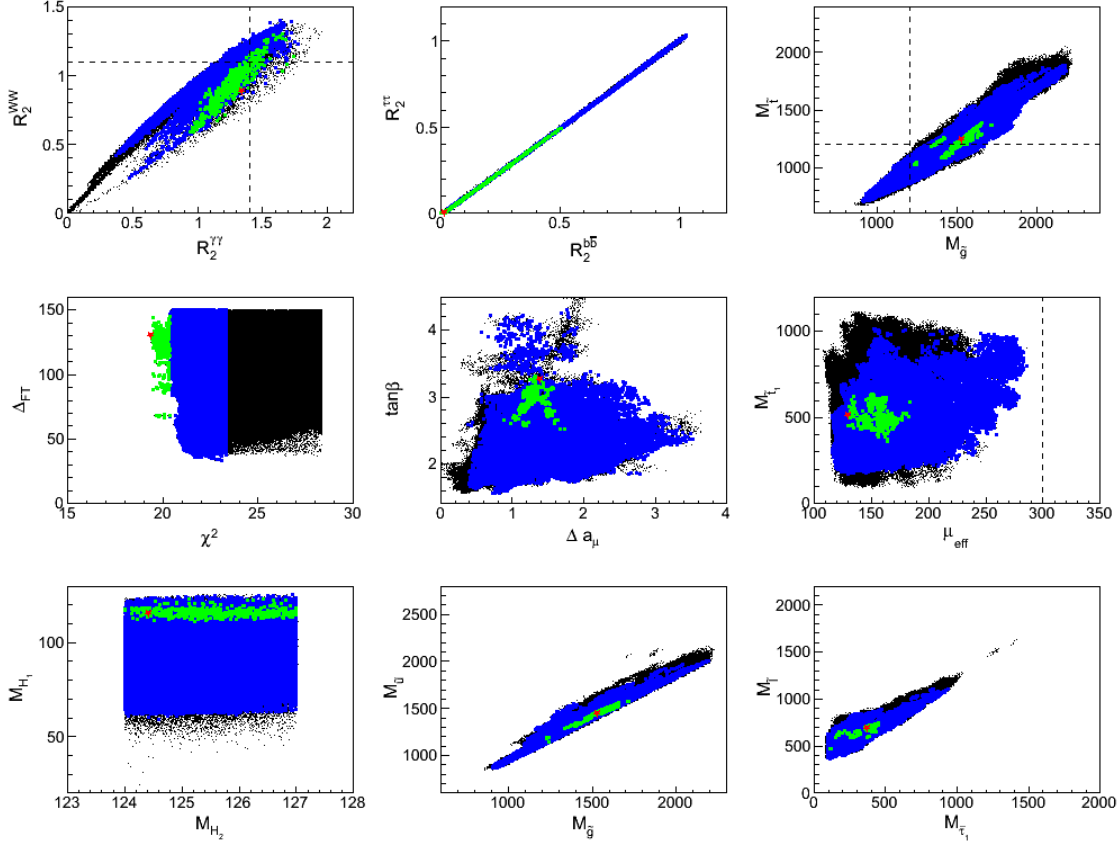


FIG. 3: The fitting results for Scenario II with relic density smaller than the 95% C.L. upper limit. The red stars show the best-fitted benchmark point with minimal $\chi^2_{min} = 19.35$. The green, blue, and black regions are respectively one, two, and three standard deviation regions with $\chi^2 < \chi^2_{min} + 1$, $\chi^2_{min} + 4$, and $\chi^2_{min} + 9$.

can evade the LHC supersymmetry search and XENON100 experiment constraints, and the R -parity violation superpotential term(s) may increase $(g_\mu - 2)/2$ and explain the neutrino masses and mixings. Therefore, Scenario III with R -parity violation is more natural and realistic than Scenarios I and II.

Acknowledgments

We would like to thank Zhaofeng Kang and Chunli Tong for collaboration in the early stage of this project. This research was supported in part by the Natural Science Foundation of China under grant numbers 11075003, 10821504, 11075194, and 11135003, by the

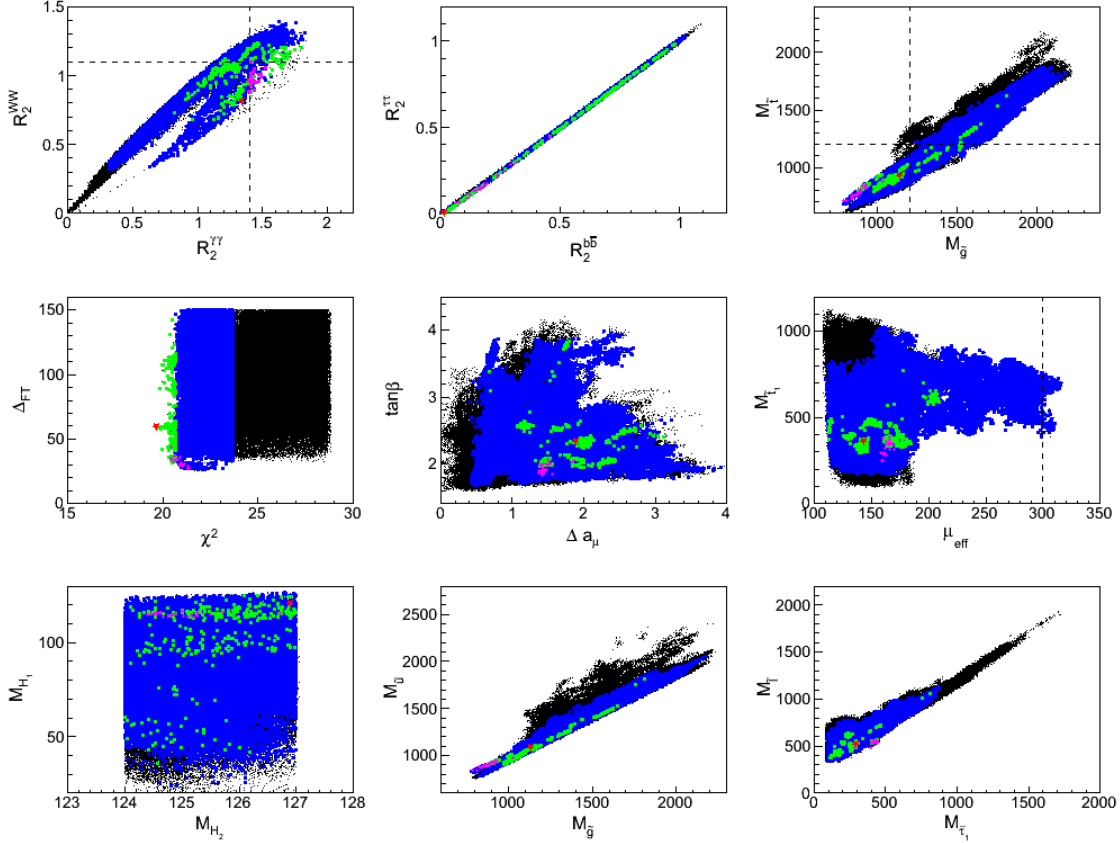


FIG. 4: The fitting results for Scenario III without R -parity. The red stars show the best-fitted benchmark point with minimal $\chi^2_{min} = 19.67$. The green, blue, and black regions are respectively one, two, and three standard deviation regions with $\chi^2 < \chi^2_{min} + 1$, $\chi^2_{min} + 4$, and $\chi^2_{min} + 9$. The magenta region corresponds to $R_{\gamma\gamma} > 1.4$, $R_{VV} < 1.1$, $R_{bb} < 1.0$, $R_{\tau\tau} < 1.0$, $M_{\tilde{t}} = \sqrt{m_{\tilde{t}_1}^2 + m_{\tilde{t}_2}^2} < 1.2\text{TeV}$, $\mu_{\text{eff}} < 300\text{ GeV}$, $M_{\tilde{g}} < 1.2\text{ TeV}$, $\chi^2 < \chi^2_{min} + 4$, and $\Delta_{\text{FT}} < 50$.

Postdoctoral Science Foundation of China under grant number Y2Y2231B11, and by the DOE grant DE-FG03-95-Er-40917.

-
- [1] J. R. Ellis, S. Kelley and D. V. Nanopoulos, Phys. Lett. B **249**, 441 (1990); Phys. Lett. B **260**, 131 (1991); U. Amaldi, W. de Boer and H. Furstenau, Phys. Lett. B **260**, 447 (1991); P. Langacker and M. X. Luo, Phys. Rev. D **44**, 817 (1991); F. Anselmo, L. Cifarelli, A. Peterman and A. Zichichi, Nuovo Cim. A **104**, 1817 (1991); Nuovo Cim. A **105**, 1025 (1992).

- [2] J. R. Ellis, J. S. Hagelin, D. V. Nanopoulos and M. Srednicki, Phys. Lett. B **127**, 233 (1983);
J. R. Ellis, J. S. Hagelin, D. V. Nanopoulos, K. A. Olive and M. Srednicki, Nucl. Phys. B **238**, 453 (1984).
- [3] H. Goldberg, Phys. Rev. Lett. **50**, 1419 (1983) [Erratum-ibid. **103**, 099905 (2009)].
- [4] G. Aad *et al.* [ATLAS Collaboration], arXiv:1109.6572 [hep-ex].
- [5] G. Aad *et al.* [ATLAS Collaboration], JHEP **1111**, 099 (2011) [arXiv:1110.2299 [hep-ex]].
- [6] S. Chatrchyan *et al.* [CMS Collaboration], Phys. Rev. Lett. **107**, 221804 (2011) [arXiv:1109.2352 [hep-ex]].
- [7] The ATLAS Collaboration, ATLAS-CONF-2012-033; ATLAS-CONF-2012-037; The CMS Collaboration, CMS-PAS-SUS-11-004.
- [8] For a recent review, see A. Parker, talk at the 36th ICHEP, Melbourne, Australia, July 2012.
- [9] J. Incandela [on behalf of CMS], “Status of the CMS SM Higgs Search”, and F. Gianotti [on behalf of ATLAS], “Status of the SM Higgs Search in ATLAS”, joint CMS/ATLAS seminars at CERN on July 4, 2012.
- [10] The ATLAS Collaboration, ATLAS-CONF-2012-093; ATLAS-CONF-2012-098.
- [11] The CMS Collaboration, CMS-PAS-HIG-12-020.
- [12] L. J. Hall, D. Pinner and J. T. Ruderman, JHEP **1204**, 131 (2012) [arXiv:1112.2703 [hep-ph]]; H. Baer, V. Barger and A. Mustafayev, Phys. Rev. D **85**, 075010 (2012) [arXiv:1112.3017 [hep-ph]]; T. Li, J. A. Maxin, D. V. Nanopoulos and J. W. Walker, Phys. Lett. B **710**, 207 (2012) [arXiv:1112.3024 [hep-ph]]; S. Heinemeyer, O. Stal and G. Weiglein, Phys. Lett. B **710**, 201 (2012) [arXiv:1112.3026 [hep-ph]]; A. Arbey, M. Battaglia and F. Mahmoudi, Eur. Phys. J. C **72**, 1906 (2012) [arXiv:1112.3032 [hep-ph]]; S. Akula, B. Altunkaynak, D. Feldman, P. Nath and G. Peim, Phys. Rev. D **85**, 075001 (2012) [arXiv:1112.3645 [hep-ph]]; M. Kadastik, K. Kannike, A. Racioppi and M. Raidal, JHEP **1205**, 061 (2012) [arXiv:1112.3647 [hep-ph]]; U. Ellwanger, JHEP **1203**, 044 (2012) [arXiv:1112.3548 [hep-ph]]; O. Buchmueller, R. Cavanaugh, A. De Roeck, M. J. Dolan, J. R. Ellis, H. Flacher, S. Heinemeyer and G. Isidori *et al.*, arXiv:1112.3564 [hep-ph]; J. Cao, Z. Heng, D. Li and J. M. Yang, Phys. Lett. B **710**, 665 (2012) [arXiv:1112.4391 [hep-ph]]; J. F. Gunion, Y. Jiang and S. Kraml, Phys. Lett. B **710**, 454 (2012) [arXiv:1201.0982 [hep-ph]]; S. F. King, M. Muhlleitner and R. Nevzorov, Nucl. Phys. B **860**, 207 (2012) [arXiv:1201.2671 [hep-ph]]; Z. Kang, J. Li and T. Li, arXiv:1201.5305 [hep-ph]; C. -F. Chang, K. Cheung, Y. -C. Lin and T. -C. Yuan, JHEP

- 1206**, 128 (2012) [arXiv:1202.0054 [hep-ph]]; L. Aparicio, D. G. Cerdeno and L. E. Ibanez, JHEP **1204**, 126 (2012) [arXiv:1202.0822 [hep-ph]]; H. Baer, V. Barger and A. Mustafayev, JHEP **1205**, 091 (2012) [arXiv:1202.4038 [hep-ph]]; J. Cao, Z. Heng, J. M. Yang, Y. Zhang and J. Zhu, JHEP **1203**, 086 (2012) [arXiv:1202.5821 [hep-ph]]; Z. Kang, T. Li, T. Liu, C. Tong and J. M. Yang, arXiv:1203.2336 [hep-ph]; N. D. Christensen, T. Han and S. Su, arXiv:1203.3207 [hep-ph]; D. A. Vasquez, G. Belanger, C. Boehm, J. Da Silva, P. Richardson and C. Wymant, arXiv:1203.3446 [hep-ph]; M. A. Ajaib, I. Gogoladze, F. Nasir and Q. Shafi, arXiv:1204.2856 [hep-ph]; K. Blum, R. T. D’Agnolo and J. Fan, arXiv:1206.5303 [hep-ph]; K. Hagiwara, J. S. Lee and J. Nakamura, arXiv:1207.0802 [hep-ph].
- [13] M. Carena, S. Gori, N. R. Shah and C. E. M. Wagner, arXiv:1112.3336 [hep-ph]; M. Carena, S. Gori, N. R. Shah, C. E. M. Wagner and L. -T. Wang, arXiv:1205.5842 [hep-ph].
- [14] U. Ellwanger and C. Hugonie, arXiv:1203.5048 [hep-ph].
- [15] A. Albaid and K. S. Babu, arXiv:1207.1014 [hep-ph]; T. Li, J. A. Maxin, D. V. Nanopoulos and J. W. Walker, arXiv:1207.1051 [hep-ph]; R. Benbrik, M. G. Bock, S. Heinemeyer, O. Stal, G. Weiglein and L. Zeune, arXiv:1207.1096 [hep-ph]; A. Arbey, M. Battaglia, A. Djouadi and F. Mahmoudi, arXiv:1207.1348 [hep-ph]; J. Ellis and T. You, arXiv:1207.1693 [hep-ph]. S. Akula, P. Nath and G. Peim, arXiv:1207.1839 [hep-ph]; H. An, T. Liu and L. -T. Wang, arXiv:1207.2473 [hep-ph]; B. Kyae and J. -C. Park, arXiv:1207.3126 [hep-ph]; H. Baer, V. Barger, P. Huang, A. Mustafayev and X. Tata, arXiv:1207.3343 [hep-ph]; J. Cao, Z. Heng, J. M. Yang and J. Zhu, arXiv:1207.3698 [hep-ph].
- [16] J. F. Gunion, Y. Jiang and S. Kraml, arXiv:1207.1545 [hep-ph].
- [17] Tevatron New Physics Higgs Working Group and CDF and D0 Collaborations, arXiv:1207.0449 [hep-ex].
- [18] R. D. Peccei and H. R. Quinn, Phys. Rev. Lett. **38** (1977) 1440; Phys. Rev. **D16** (1977) 1791.
- [19] S. Weinberg, Phys. Rev. Lett. **40** (1978) 223; F. Wilczek, Phys. Rev. Lett. **40** (1978) 279.
- [20] For reviews see: J. E. Kim, Phys. Rep. **150** (1987) 1; H. Y. Cheng, Phys. Rep. **158** (1988) 1; M. S. Turner, Phys. Rep. **197** (1991) 67; G. G. Raffelt, Phys. Rep. **333** (2000) 593; G. Gabadadze and M. Shifman, Int. J. Mod. Phys. **A17** (2002) 3689.
- [21] J. E. Kim, Phys. Rev. Lett. **43** (1979) 103; M. Shifman, A. Vainshtein, V. Zakharov, Nucl. Phys. **B166** (1980) 493.
- [22] A. R. Zhitnitskii, Sov. J. Nucl. Phys. **31** (1980) 260; M. Dine, W. Fischler, M. Srednicki, Phys.

- Lett. **B104** (1981) 199.
- [23] E. Aprile *et al.* [XENON100 Collaboration], Phys. Rev. Lett. **107**, 131302 (2011) [arXiv:1104.2549 [astro-ph.CO]]; E. Aprile, M. Alfonsi, K. Arisaka, F. Arneodo, C. Balan, L. Baudis, A. Behrens and P. Beltrame *et al.*, arXiv:1207.3458 [astro-ph.IM].
 - [24] R. Barbier, C. Berat, M. Besancon, M. Chemtob, A. Deandrea, E. Dudas, P. Fayet and S. Lavignac *et al.*, Phys. Rept. **420**, 1 (2005) [hep-ph/0406039].
 - [25] E. Nikolidakis and C. Smith, Phys. Rev. D **77**, 015021 (2008) [arXiv:0710.3129 [hep-ph]]; C. Csaki, Y. Grossman and B. Heidenreich, Phys. Rev. D **85**, 095009 (2012) [arXiv:1111.1239 [hep-ph]].
 - [26] J. Beringer *et al.* (Particle Data Group), Phys. Rev. D **86**, 010001 (2012).
 - [27] J. R. Ellis, K. Enqvist, D. V. Nanopoulos and F. Zwirner, Mod. Phys. Lett. A **1**, 57 (1986); R. Barbieri and G. F. Giudice, Nucl. Phys. B **306**, 63 (1988).
 - [28] R. Kitano and Y. Nomura, Phys. Lett. B **631**, 58 (2005) [hep-ph/0509039]; Phys. Rev. D **73**, 095004 (2006) [hep-ph/0602096].
 - [29] M. Papucci, J. T. Ruderman and A. Weiler, arXiv:1110.6926 [hep-ph].
 - [30] H. K. Dreiner, M. Hanussek and C. Luhn, arXiv:1206.6305 [hep-ph].
 - [31] P. N. Pandita and P. F. Paulraj, Phys. Lett. B **462**, 294 (1999) [hep-ph/9907561]; P. N. Pandita, Phys. Rev. D **64**, 056002 (2001) [hep-ph/0103005].
 - [32] D. E. Lopez-Fogliani and C. Munoz, Phys. Rev. Lett. **97**, 041801 (2006) [hep-ph/0508297]; N. Escudero, D. E. Lopez-Fogliani, C. Munoz and R. R. de Austri, JHEP **0812**, 099 (2008) [arXiv:0810.1507 [hep-ph]]; K. -Y. Choi, D. E. Lopez-Fogliani, C. Munoz and R. R. de Austri, JCAP **1003**, 028 (2010) [arXiv:0906.3681 [hep-ph]]; J. Fidalgo, D. E. Lopez-Fogliani, C. Munoz and R. R. de Austri, JHEP **1110**, 020 (2011) [arXiv:1107.4614 [hep-ph]].
 - [33] U. Ellwanger and C. Hugonie, Comput. Phys. Commun. **177**, 399 (2007) [hep-ph/0612134]; Comput. Phys. Commun. **175**, 290 (2006) [hep-ph/0508022]; U. Ellwanger, J. F. Gunion and C. Hugonie, JHEP **0502**, 066 (2005) [hep-ph/0406215].
 - [34] D. Larson, J. Dunkley, G. Hinshaw, E. Komatsu, M. R.olta, C. L. Bennett, B. Gold and M. Halpern *et al.*, Astrophys. J. Suppl. **192**, 16 (2011) [arXiv:1001.4635 [astro-ph.CO]].

Point	$\text{I}\chi^2_{\min}$	IA	IB	IC	Point	$\text{I}\chi^2_{\min}$	IA	IB	IC
M_0	264	294	562	249	\tilde{t}_1	294	210	186	257
$M_{1/2}$	489	484	624	571	\tilde{t}_2	822	810	1026	920
$\tan\beta$	2.436	2.851	2.910	3.293	\tilde{t}	873	837	1042	955
λ	0.601	0.550	0.564	0.536	\tilde{b}_1	783	768	994	880
κ	0.245	0.249	0.268	0.243	\tilde{b}_2	983	979	1296	1114
A_0	-1180	-1253	-1779	-1441	\tilde{u}_R/\tilde{c}_R	1053	1052	1397	1197
A_λ	-315	-230	-628	-193	\tilde{u}_L/\tilde{c}_L	1059	1057	1398	1206
A_κ	-1.904	-2.028	-218.408	-1.900	\tilde{d}_R/\tilde{s}_R	1014	1013	1342	1153
μ_{eff}	130	124	123	128	\tilde{d}_L/\tilde{s}_L	1061	1059	1399	1208
M_1	207	204	266	242	H_1^0	108.5	95.5	111.7	91.7
M_2	384	380	493	449	H_2^0	125.5	125.4	125.2	124.2
M_3	1091	1081	1368	1259	H_3^0	359.7	396.3	385.6	461.1
$\tilde{\chi}_1^0$	75	70	77	76	A_1	99.6	123.8	91.7	138.4
$\tilde{\chi}_2^0$	163	-156	-156	-158	A_2	353.4	390.0	377.9	455.9
$\tilde{\chi}_3^0$	-168	163	172	171	H^\pm	343.9	383.2	371.3	450.2
$\tilde{\chi}_4^0$	219	216	273	250	Ωh^2	0.110	0.104	0.103	0.109
$\tilde{\chi}_5^0$	415	410	521	475	$\Delta_{a_\mu} [10^{-10}]$	2.317	2.586	1.157	1.823
$\tilde{\chi}_1^\pm$	114	109	113	117	$\sigma^{si}(p) [10^{-10} \text{ pb}]$	7.468	1.137	3.208	39.683
$\tilde{\chi}_2^\pm$	414	409	520	475	$\text{Br}^{(b \rightarrow s\gamma)} [10^{-4}]$	3.342	2.633	2.714	2.747
\tilde{g}	1134	1125	1436	1305	Δ_{FT}	62.7	74.0	109.3	101.5
$\tilde{\nu}_{e/\mu}$	457	472	741	497	$R_2^{\gamma\gamma}_{\text{VBF}}$	1.48	1.60	1.75	1.46
$\tilde{\nu}_\tau$	456	471	740	496	$R_2^{\gamma\gamma}$	1.58	1.43	1.45	1.31
$\tilde{e}_R/\tilde{\mu}_R$	178	216	482	126	R_2^{WW}	1.25	1.10	1.07	1.09
$\tilde{e}_L/\tilde{\mu}_L$	461	477	744	502	R_2^{ZZ}	1.25	1.10	1.07	1.09
$\tilde{\tau}_1$	176	213	479	116	R_2^{Vbb}	0.59	0.59	0.50	0.70
$\tilde{\tau}_2$	461	476	744	501	R_2^{bb}	0.63	0.53	0.41	0.63
χ^2	21.16	24.85	25.92	23.37	$R_2^{\tau\tau}$	0.62	0.53	0.41	0.62

TABLE IV: Particle spectra (in GeV) and parameters for benchmark points in Scenario I.

Point	$\text{II}\chi_{min}^2$	IIA	IIB	IIC	Point	$\text{II}\chi_{min}^2$	IIA	IIB	IIC
M_0	454	208	576	279	\tilde{t}_1	513	157	184	432
$M_{1/2}$	673	413	528	527	\tilde{t}_2	1126	700	912	895
$\tan\beta$	3.267	2.518	2.468	1.820	\tilde{t}	1237	717	930	994
λ	0.452	0.617	0.582	0.584	\tilde{b}_1	1093	654	880	866
κ	0.214	0.295	0.247	0.172	\tilde{b}_2	1348	835	1153	1058
A_0	-1520	-1090	-1519	-986	\tilde{u}_R/\tilde{c}_R	1434	898	1240	1127
A_λ	-296	-248	-618	-380	\tilde{u}_L/\tilde{c}_L	1445	903	1237	1135
A_κ	-1.354	-1.049	-253.408	-1.707	\tilde{d}_R/\tilde{s}_R	1384	865	1192	1086
μ_{eff}	130	129	118	123	\tilde{d}_L/\tilde{s}_L	1446	905	1239	1136
M_1	287	173	224	224	H_1^0	115.2	106.5	99.7	98.0
M_2	530	324	416	416	H_2^0	124.4	126.2	124.7	126.0
M_3	1467	933	1169	1173	H_3^0	440.5	363.1	332.7	290.1
$\tilde{\chi}_1^0$	87	70	69	74	A_1	66.1	145.4	103.3	74.6
$\tilde{\chi}_2^0$	-152	-166	-156	133	A_2	435.0	355.4	325.3	288.4
$\tilde{\chi}_3^0$	167	170	158	-166	H^\pm	433.6	345.6	316.3	275.7
$\tilde{\chi}_4^0$	292	194	233	233	Ωh^2	0.038	0.001	0.072	0.070
$\tilde{\chi}_5^0$	557	358	446	444	$\Delta_{a_\mu} [10^{-10}]$	1.385	3.410	1.100	1.513
$\tilde{\chi}_1^\pm$	122	107	104	107	$\sigma^{si}(p) [10^{-10} \text{ pb}]$	59.671	39.947	22.116	28.064
$\tilde{\chi}_2^\pm$	556	357	446	444	$\text{Br}^{(b \rightarrow s\gamma)} [10^{-4}]$	3.553	2.294	2.914	4.123
\tilde{g}	1529	968	1235	1218	Δ_{FT}	130.4	48.8	75.7	59.6
$\tilde{\nu}_{e/\mu}$	680	377	710	489	$R_{2\text{VBF}}^{\gamma\gamma}$	1.08	1.68	1.53	1.24
$\tilde{\nu}_\tau$	679	377	709	489	$R_2^{\gamma\gamma}$	1.34	1.45	1.42	1.42
$\tilde{e}_R/\tilde{\mu}_R$	376	122	510	191	R_2^{WW}	0.89	1.09	1.10	1.09
$\tilde{e}_L/\tilde{\mu}_L$	683	383	713	492	R_2^{ZZ}	0.89	1.09	1.10	1.09
$\tilde{\tau}_1$	372	118	509	190	R_2^{Vbb}	0.01	0.57	0.72	0.65
$\tilde{\tau}_2$	683	383	712	492	R_2^{bb}	0.01	0.49	0.67	0.74
χ^2	19.35	24.19	23.86	23.70	$R_2^{\tau\tau}$	0.00	0.49	0.66	0.73

TABLE V: Particle spectra (in GeV) and parameters for benchmark points in Scenario II.

Point	III χ^2_{min}	IIIA	IIIB	IIIC	Point	III χ^2_{min}	IIIA	IIIB	IIIC
M_0	352	431	344	337	\tilde{t}_1	365	252	184	391
$M_{1/2}$	489	326	500	441	\tilde{t}_2	850	647	832	795
$\tan \beta$	2.341	1.853	2.731	2.039	\tilde{t}	925	694	852	886
λ	0.604	0.589	0.623	0.614	\tilde{b}_1	814	610	793	760
κ	0.295	0.364	0.288	0.318	\tilde{b}_2	1012	778	1020	929
A_0	-1063	-372	-1322	-620	\tilde{u}_R/\tilde{c}_R	1078	827	1097	985
A_λ	-329	-161	-267	-9.93×10^{-6}	\tilde{u}_L/\tilde{c}_L	1083	823	1101	990
A_κ	-128.134	-628.214	-0.877	-1.459	\tilde{d}_R/\tilde{s}_R	1039	798	1056	952
μ_{eff}	144	162	150	166	\tilde{d}_L/\tilde{s}_L	1085	825	1103	992
M_1	207	136	212	186	H_1^0	120.5	114.3	119.6	116.6
M_2	384	255	393	346	H_2^0	126.9	124.6	124.9	125.7
M_3	1090	745	1114	990	H_3^0	367.8	342.7	436.6	382.5
$\tilde{\chi}_1^0$	91	86	92	107	A_1	154.3	300.6	157.1	247.6
$\tilde{\chi}_2^0$	-177	160	-184	195	A_2	360.0	335.1	430.1	376.3
$\tilde{\chi}_3^0$	187	-189	191	-197	H^\pm	352.6	330.2	421.7	369.3
$\tilde{\chi}_4^0$	222	232	228	221	Ωh^2	\times	\times	\times	\times
$\tilde{\chi}_5^0$	417	310	425	384	$\Delta_{a_\mu} [10^{-10}]$	1.893	1.587	2.207	1.848
$\tilde{\chi}_1^\pm$	126	122	133	141	$\sigma^{si}(p) [10^{-10} \text{ pb}]$	\times	\times	\times	\times
$\tilde{\chi}_2^\pm$	416	306	425	383	$\text{Br}^{(b \rightarrow s\gamma)} [10^{-4}]$	3.586	3.413	2.560	3.659
\tilde{g}	1138	796	1162	1035	Δ_{FT}	59.5	27.0	68.4	44.1
$\tilde{\nu}_{e/\mu}$	513	502	514	475	$R_{2\text{VBF}}^{\gamma\gamma}$	0.88	0.93	1.60	1.16
$\tilde{\nu}_\tau$	512	502	514	475	$R_2^{\gamma\gamma}$	1.34	1.46	1.41	1.42
$\tilde{e}_R/\tilde{\mu}_R$	291	395	273	289	R_2^{WW}	0.81	0.95	1.08	1.10
$\tilde{e}_L/\tilde{\mu}_L$	517	505	519	479	R_2^{ZZ}	0.81	0.95	1.08	1.10
$\tilde{\tau}_1$	289	395	270	288	R_2^{Vbb}	0.01	0.10	0.55	0.37
$\tilde{\tau}_2$	517	505	518	479	R_2^{bb}	0.02	0.16	0.48	0.46
χ^2	19.67	21.31	23.85	20.53	$R_2^{\tau\tau}$	0.00	0.14	0.47	0.44

TABLE VI: Particle spectra (in GeV) and parameters for benchmark points in Scenario III.